Fabrication of electrospun polymer nanofibers modified with all-inorganic perovskite nanocrystals for flexible optoelectronic devices

Muhammad Ahmad Bkkar[1] · **Roman Olegovich Olekhnovich[2]** · **Arina Valerievna Kremleva[3]** · **Yakov Nikolaevich Kovach[3]** · **Victoria Kalanchina[1]** · **Mayya Valerievna Uspenskaya[1]**

Abstract

Polymer–perovskite nanofibers are considered promising active nanomaterials for flexible optoelectronic devices. Herein, polyvinylpyrrolidone (PVP) nanofibers modified with black-phase cesium lead iodide ($CsPbI_3$) nanocrystals (NCs) have been prepared by a one-stage electrospinning method followed by an annealing process. The average diameter of drop-free nanofibers has been varied in the range of 81–579 nm by manipulating the concentration of the entire material from 47.39% to 41.39%; the concentration of perovskite from 33.33% to 46.67%; the concentration of PVP from 7.5% to 15%; the needle diameter from 0.42 mm to 0.72 mm; the feed rate from 0.1 ml/h to 0.3 ml/h; the electrical voltage from 17 to 23 kV; and the working distance from 120 to 150 mm. The correlation between properties of solutions (viscosity of 87–2949 mPa s, electrical conductivity of 5.41–8.44 mS/cm, and surface tension of 38.98–42.66 mN/m) and the average diameter has been described. Stable NCs embedded in PVP nanofibers are obtained after 5 min of annealing at 150–200 °C. Light absorption and photoluminescence (PL) properties improve with an increase in the annealing temperature from 150 °C to 200 °C due to the growth in grain size. The optical bandgap has been found to be ~ 1.77 eV and 1.74 eV at 150 °C and 200 °C, respectively. The formation mechanism of stable NCs has been presented. The low annealing temperature can be explained by the formation of ionic clusters and the aggregation of perovskite precursors around the polymer chains in the intermediate phase, promoting the non-classical nucleation. The stability at room conditions is attributed to the small size of crystals and their complexation with PVP, which allows the fabrication of stable nanofibers for 15 days.

Keywords Nanofibers · Polymer · Perovskite · Crystallinity · Complexation · Stability

Introduction

Nowadays, the need for flexible light-weight photoactive layers is urgent to fabricate wearable and building integrated optoelectronic devices. Electrospun nanofibers (ENfs) are considered hopeful one-dimensional nanostructured materials for devices of this type, owning to their unique properties, such as low weight, adjustable surface properties, flexibility, large specific surface area, and low cost (Ding and Yu 2014; He et al. 2008; Ahmadian et al. 2021; Wang et al. 2021a; Sarac 2017; Bohr et al. 2022). Recently, the one-stage electrospinning process has attracted researchers

✉ Muhammad Ahmad Bkkar
  mbkkar@itmo.ru

  Roman Olegovich Olekhnovich
  r.o.olekhnovich@mail.ru

  Arina Valerievna Kremleva
  avkremleva@itmo.ru

  Yakov Nikolaevich Kovach
  yakovachyakov@gmail.com

  Victoria Kalanchina
  kalanchina2020@mail.ru

  Mayya Valerievna Uspenskaya
  mv_uspenskaya@itmo.ru

[1] Chemical Engineering Center, ITMO University, Saint-Petersburg 197101, Russia

[2] Faculty of Control Systems and Robotics, ITMO University, Saint-Petersburg 197101, Russia

[3] Institute of Advanced Data Transfer System, ITMO University, Saint-Petersburg 197101, Russia

to fabricate polymer nanofibers, modified with perovskite crystals using two different strategies (Zhang et al. 2020a; Chen et al. 2021; Bohr et al. 2019; Chen and Zhu 2017; Li et al. 2019; Kim et al. 2022; Bkkar et al. 2020). The first strategy (pre-crystallization of perovskite outside fibers PPOF) depends on electrospinning polymer solutions containing perovskite NCs or quantum dots (QDs), e.g., γ-cesium lead bromide (γ-$CsPbBr_3$):polymethyl methacrylate (PMMA) (Zhang et al. 2020a), $CsPbBr_3$:polystyrene (PS) (Chen et al. 2021). Whereas the second strategy (crystallization of perovskite into fibers CPIF) depends on electrospinning polymer solutions containing perovskite precursors followed by an annealing process, e.g., methylammonium lead iodide ($MAPbI_3$)–PVP (Bohr et al. 2019; Chen and Zhu 2017), $MAPbI_3$–polyacrylonitrile (PAN) (Li et al. 2019), $MAPbI_3$–PVP (Kim et al. 2022). Actually, the second method is simpler and cheaper, since the first one is limited by additional costs of perovskite NCs or QDs synthesis and their easy decomposition in polar solvents (Wang et al. 2021b; Akkerman et al. 2018; Sun et al. 2021). In the second strategy, $MAPbI_3$ perovskite is commonly used to fabricate composite nanofibers due to its desirable optoelectronic properties (Bohr et al. 2019; Chen and Zhu 2017; Li et al. 2019; Kim et al. 2022). However, the low thermal and moisture stability of $MAPbI_3$ has restricted the future development and mass production of this type of nanofibers (Ava et al. 2019),Tumusange et al. (Tumusange et al. 2021). Organic-free $CsPbI_3$ perovskite is considered an optimal alternative for organic–inorganic halide perovskites. It possesses high thermal stability, a light absorption spectrum up to 700 nm, and long carrier diffusion lengths (Yao et al. 2021a, 2021b; Miyasaka et al. 2020; Masi et al. 2020). This perovskite has three black crystalline phases (α, β, γ) and a yellow phase (δ). To prepare the cubic black-phase α-$CsPbI_3$, an annealing process at a temperature of above 300 °C is required. By cooling, this structure changes to the tetragonal black phase (β-$CsPbI_3$) at a temperature of about 260 °C, then to the orthorhombic black phase (γ-$CsPbI_3$) at a temperature of about 175 °C, and finally to the orthorhombic yellow phase (δ-$CsPbI_3$) at room temperature (Yao et al. 2021a, 2021b; Miyasaka et al. 2020; Masi et al. 2020). The degradation of black-phase $CsPbI_3$ at low temperatures is mainly ascribed to the small cation Cs^+ that cannot maintain the cubic framework of $[PbI_6]^{-4}$ (Yao et al. 2021a, 2021b; Miyasaka et al. 2020; Masi et al. 2020). Thus, it is a challenge to improve the thermodynamic stability of $CsPbI_3$ at room temperature. Various approaches, such as composition engineering (Cao et al. 2019; Wang et al. 2021c; Liu et al. 2021; Patil et al. 2020), additive engineering (Yi et al. 2020; Li et al. 2018),Bansode et al. (Bansode et al. 2019) and crystal engineering (Yao et al. 2021a, 2021b; Miyasaka et al. 2020; Masi et al. 2020; Li et al. 2018; Bansode et al. 2019; Wang et al. 2021d, 2018; Haque et al. 2018) have been

used to ameliorate problems related to $CsPbI_3$. Composition engineering is dependent on modifying the tolerance factor by A site doping (A cation: cesium, methylammonium, formamidinium, etc.) (Cao et al. 2019), B site doping (B metal: lead, tin, etc.) (Wang et al. 2021c; Liu et al. 2021), and/or X site doping (X halide: iodide, bromide, chloride) (Wang et al. 2021c; Patil et al. 2020) to improve the thermodynamic phase stability of ABX_3 perovskite. Additive engineering leads to a lower annealing temperature and increased stability at room conditions, which can be explained by interactive relationships between perovskite and additives, i.e., the formation of an intermediate phase (Yi et al. 2020), the passivation effect (Li et al. 2018), as well as the restriction of crystal growth (Li et al. 2018),Bansode et al. (Bansode et al. 2019). Crystal engineering aims to reduce grain size by preparing QDs or NCs (Yao et al. 2021a, 2021b; Miyasaka et al. 2020; Masi et al. 2020; Wang et al. 2021d), or controlling the crystallization rate of perovskite (Yao et al. 2021a, 2021b; Miyasaka et al. 2020; Masi et al. 2020; Yi et al. 2020; Li et al. 2018; Bansode et al. 2019; Wang et al. 2021d, 2018; Haque et al. 2018). The high surface to volume ratio increases the structural stability of perovskite (Yao et al. 2021a, 2021b; Miyasaka et al. 2020; Masi et al. 2020; Li et al. 2018; Wang et al. 2021d). The crystallization rate can be strictly controlled by annealing and additive engineering (Li et al. 2018),Bansode et al. (Bansode et al. 2019; Haque et al. 2018),Wang et al. (Wang et al. 2018). Herein, we have used the CPIF strategy to fabricate flexible PVP nanofibers containing stable black-phase $CsPbI_3$ NC_S by integrating the one-stage electrospinning process with additive and crystal engineering. The one-stage electrospinning process has been used to prepare nanofibers. Various parameters associated with this process have been studied to produce high-quality electrospun membranes. PVP was used as an electrospinnable polymer to promote obtaining ENFs and as an additive to support stable perovskite at room temperature. The annealing process was utilized to control crystal size. The passivation effect of the polymer and the small size of crystals increase the stability of $CsPbI_3$ at room temperature.

Experimental section

Materials

Cesium iodide (CsI, 99.9%) and lead (II) iodide (PbI_2, 99.5%) were purchased from (Chemcraft, Russia). Anhydrous dimethylformamide (DMF, 99.8%) and polyvinylpyridine (PVP, Mw 1,300,000) were purchased from (Sigma-Aldrich, Germany). Glass substrates were purchased from (Medtechnika 7, Russia).

Methods

Preparation of electrospinning solutions The electrospinning solution was obtained by dissolving PVP in DMF with stirring for 5 min by a magnetic stirrer at a rotational speed of 300 rpm. Then, perovskite salts (i.e., CsI and PbI$_2$) were added to the polymer solution. To get a homogeneous solution, the mixture was stirred for 60 min at a rotational speed of 600 rpm. The solution was made at a temperature of 27 °C and humidity of 21% (room conditions). The electrospinning solution was manipulated by changing the amount of DMF to vary the concentration of the total material in the range of 55.25–41.39%, the amount of perovskite from 6.98% to 46.67%, or the amount of PVP from 5 to 15%. Electrospinning solutions and results are listed in Table 1.

Fabrication of composite ENfs CsPbI$_3$:PVP nanofibers were produced by a one-stage electrospinning method. Various technological parameters were tested, i.e., a needle diameter of 0.34–0.92 mm, a solution feed rate of 0.1–1 ml/h, a working distance of 50–150 mm, and an applied voltage of 10–30 kV. The resulting electrospinning solution with a volume of 2–3 ml was loaded into a 5 ml syringe of the electrospinning machine (Nanon 01A) at room conditions (a temperature of 27 °C and humidity of 21%). A tubeless spinneret has been used.

Cleaning substrates Substrates were cleaned by an ultrasonic bath UZV7/100-TH (22 kHz, 40 °C) in water, acetone, and isopropanol for 25 min each, then dried in an oven for 2 h at 200 °C.

Measuring the diameter of nanofibers The average diameter was calculated as the arithmetic mean of 400 PVP:CsPbI$_3$ nanofibers from 8 spots. The diameter of nanofibers was determined by specialized software Image J.

Annealing process Nanofibers on substrates were controlled by manipulating the time of the electrospinning process. The resulting nanofibers were annealed in a laboratory oven at a temperature of 60–350 °C for a period of 5–15 min.

Characterization

A scanning electron microscope MIRA3 TESCAN, an optical microscope MICROMED with immersion oil, and an OLYMPUS STM 6 microscope were used to analyze the morphology of nanofibers. The viscosity of electrospinning solutions was determined by Rheometer Physica MCR 502 (Anton Paar GmBH, Australia). Surface tension values of electrospinning solutions were determined by DSA 100 (Kruss, Germany) and their conductivity using a WTW InoLab Cond 720 conductometer with a Tetracon 325 sensor (WTW, Germany). The XRD patterns of the samples were studied using a DRON-8 X-ray setup in a slit configuration with a BSV-29 sharp-focus tube with a copper anode, a NaI (Tl) scintillation detector, and a β-filter (Ni). Fourier transform infrared (FTIR) spectra of samples were obtained

Table 1 Used electrospinning solutions

Variable component	Electrospinning solution number	PVP concentration in DMF, w/w%	Material concentration in the polymer solution, w/w%	Perovskite concentration in the polymer solution, w/w%	Electrospinning results
DMF	1	10–6	55.25	50.28–37.66	Nfs + drops
	2		50.79		Nfs + drops
	3 (ref. solution)		47.39		Nfs
	4		45.54		Nfs
	5		43.58		Nfs
	6		41.39		Nfs
Perovskite	7	7.5	13.95–50.67	6.98	drops
	8			20	Nfs + drops
	9			27.27	Nfs + drops
	10			33.33	Nfs
	11			38.46	Nfs
	(ref. solution)			43.13	Nfs
	12			46.67	Nfs
PVP	13	5	46.56–49.91	43.81–41.06	Nfs + drops
	14	6			Nfs + drops
	(ref. solution)	7.5			Nfs
	15	10			Nfs
	16	12.5			Nfs
	17	15			Nfs

by Tensor 37 (Bruker, Germany). Light absorption spectra were obtained by a setup consisting of a spectrometer [photonic multichannel analyzer PMA-12 (Hamamatsu)] and an integrating sphere (Everfine, 0.5 m) with a multi-photometer Photo-2000Z. Agilent Cary Eclipse was used to obtain PL Spectra. The thermogravimetric analysis was carried out by TG 209 F1 Libra, NETZSCH.

Results and discussion

Influence of electrospinning parameters on the quality of membranes

As is known, the performance of perovskite optoelectronic devices is crucially dependent on the crystallinity and morphology of the perovskite layer, i.e., grain size, oriented high-quality crystals, and layer uniformity (Bkkar et al. 2022). In the case of the electrospinning process, grain size and perovskite crystallinity are mainly affected by the average diameter of nanofibers and annealing parameters (Bohr et al. 2019; Bkkar et al. 2020; Tsai et al. 2018). Drops and beads lead to inhomogeneous properties of membranes (Borrotti et al. 2017). Therefore, quality control of nanofibrillar membranes (i.e., mean diameter value, unevenness in the diameter, density of drops and beads) is crucial to obtain high-efficiency flexible optoelectronic devices. There are various related parameters (e.g., setup parameters, solution parameters, and surrounding environmental conditions) that can influence the quality of membranes (Ding and Yu 2014; He et al. 2008; Ahmadian et al. 2021), and thus, affect their final structure after the annealing process (Bohr et al. 2019; Bkkar et al. 2020). Here, the influence of electrospinning parameters, including the concentration of the solution and the electrospinning setup parameters, on the average diameter value, the non-uniformity in the diameter, as well as the density of drops and beads, has been studied.

Influence of solution concentration

The electrospinning process depends on the stretching of a charged jet between the tip of the needle and the collector. All electrospinning parameters must reach the desired harmony to obtain high-quality nanofibrillar membranes. This stretch is mainly affected by the concentration of the electrospinning solution. Thus, to obtain defect-free membranes, it is important to control the concentration of the solution (Borrotti et al. 2017; Haider et al. 2018). The electrospinning solution was manipulated by changing the amount of DMF to vary the concentration of the total material in the range of 55.25–41.39%, the amount of perovskite from 6.98% to 46.67%, or the amount of PVP from 5 to 15%. Electrospinning solutions and electrospinning results

are listed in Table 1. SEM images of prepared nanofibrillar membranes using various electrospinning solutions are shown in Fig. 1a–d. Drop-free membranes were obtained at a total material concentration of 47.39–41.39%. At concentrations of above 47.39%, membranes with a high drop density have been obtained. By increasing the concentration of the material, thicker and straighter nanofibers are produced. At low concentrations (solutions 6 and 5), some beaded nanofibers were observed (Fig. 1b). A gradual increase in the concentration of the perovskite or the polymer led to the disappearance of these beads. In the case of the perovskite concentration, nanofibers were observed at a perovskite concentration of above 20%. High-quality drop-free membranes were obtained at concentrations of 33.33–46.67%. Although perovskites are inspinnable, they participate in the regulation of electrospinning solution properties to get higher quality membranes. In terms of the polymer concentration, drop-free nanofibrillar membranes are obtained at a polymer concentration of 7.5–15%. High droplet density membranes are obtained at concentrations of below 7.5%. Figure S1 shows the solution concentrations at which droplet-free nanofibers are obtained. As can be seen, the low or high concentration of the electrospinning solution, whether it is controlled by DMF, perovskite, or PVP amounts, results in the formation of defective membranes. In the case of low-concentration solutions (low viscosity), the low degree of entanglement between polymer chains leads to the formation of fragmented nanofibers. While the high concentration may prevent the solution from flowing through the needle tip. In both cases, the formation of nanofibers with beads and droplets is inevitable. The change in the mean diameter of nanofibers at various concentrations of the electrospinning solution has been shown in Fig. 2a–c. The mean diameter of nanofibers has decreased from 229 to 137 nm by increasing the DMF amount, and it has increased in the range of 81–418 nm based on perovskite, and in the range of 230–579 nm based on PVP. Consequently, finer nanofibers are obtained at low concentrations (solution 6), while maintaining the concentration of perovskite at 37.66%. Noticeably, the mean diameter of nanofibers is strongly affected by the concentration of perovskite and polymer. From Fig. 2a–c, it can be noticed that the uniformity of the diameter of nanofibers decreases with increasing the solution concentration, where some micron nanofibers can be seen at high concentrations of PVP and perovskite (Fig. 1c and d).

Influence of electrospinning setup parameters

Influence of needle diameter and feed rate SEM images of obtained nanofibrillar membranes with various needle diameters and feed rates are shown in Fig. 1e–g. Nanofibers are formed in a stable process with a needle diameter in the range of 0.42–0.72 mm and a feed rate in the range of
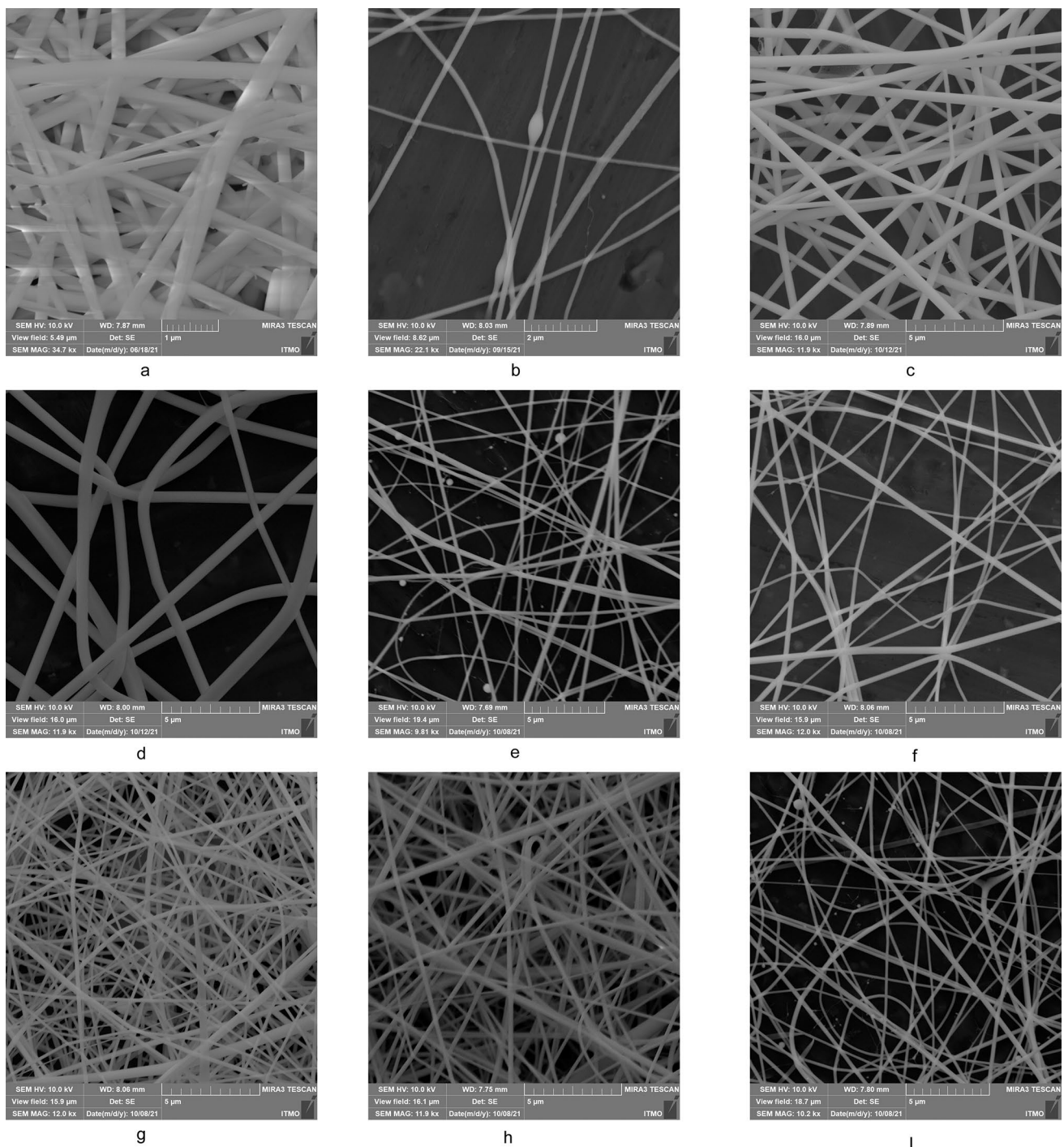
Fig. 1 SEM images of obtained nanofibers at (**a**) 23 kV electrical voltage, 0.1 ml/h feed rate, 120 mm distance, 0.42 mm needle diameter, solution 3; (**b**) 23 kV, 0.1 ml/h, 120 mm, 0.72 mm, solution 6; (**c**) 23 kV, 0.1 ml/h, 120 mm, 0.42 mm, solution 12; (**d**) 20 kV, 0.1 ml/h, 150 mm, 0.42 mm, solution 17; (**e**) 20 kV,0.1 ml/h, 120 mm, 0.72 mm, solution 6; (**f**) 20 kV, 0.1 ml/h, 120 mm, 0.42 mm, solution 6; (**g**) 23 kV, 0.3 ml/h, 120 mm, 0.72 mm, solution 6; (**h**) 23 kV,0.1 ml/h, 90 mm, 0.72 mm, solution 6; (**i**) 23 kV, 0.1 ml/h, 150 mm, 0.72 mm, solution 6

0.1–0.6 ml/h. With an increase in the feed rate from 0.4 ml/h to 0.6 ml/h, drops begin to appear in the membrane. Formed beads from low-concentration solutions (solutions 6 and 5) disappeared at low-diameter needles (0.42 mm) (Fig. 1e and

f). Also, the comparison between SEM images (Fig. 1b and g) shows that the increase in the feed rate from 0.1 ml/h to 0.3 ml/h at low solution concentrations (solution 6) leads to the disappearance of beads in the membrane. Figure 2d and e
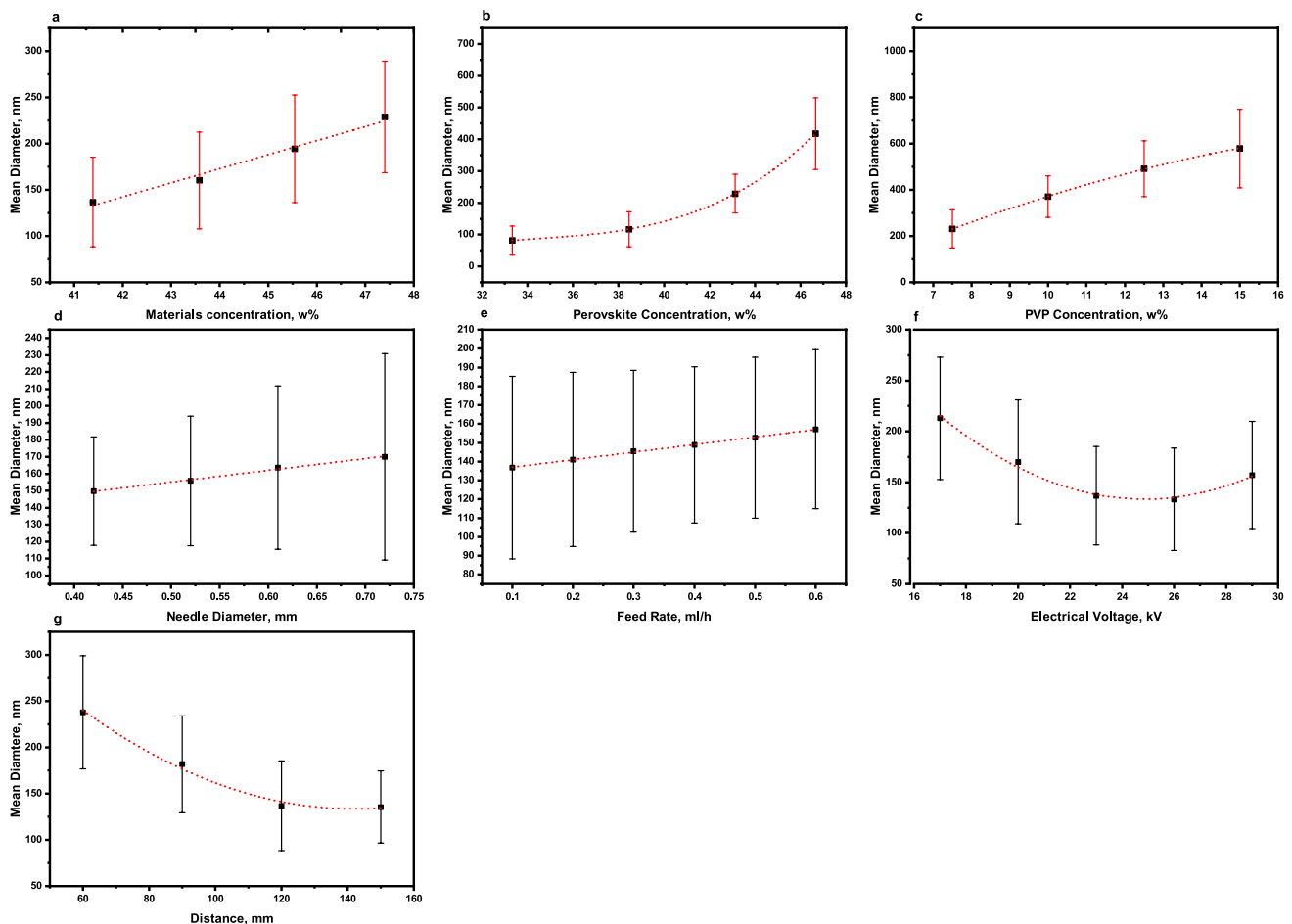
Fig. 2 The change in the mean diameter of nanofibers with the solution concentration at (**a**, **b**) 0.1 ml/h feed rate, 0.42 mm needle diameter, 23 kV voltage, 120 mm distance; (**c**) 0.1 ml/h feed rate, 0.42 mm needle diameter, 20 kV voltage, 150 mm distance. The change in the mean diameter of nanofibers with (**d**) the needle diameter at 23 kV voltage, 120 mm distance, 0.1 ml/h feed rate, solution 6; (**e**) the feed rate at 23 kV voltage, 120 mm distance, 0.72 mm needle diameter, solution 6. The change in the mean diameter of nanofibers as a function of (**f**) the working distance at 23 kV voltage, 0.1 ml/h feed rate, 0.72 mm needle diameter, solution 6; (**g**) the electric voltage at 120 mm distance, 0.1 ml/h feed rate, 0.72 mm needle diameter, solution 6

shows the change in the average diameter of nanofibers with the diameter of the needle and feed rate. With a decrease in the diameter of the needle, the average diameter of nanofibers also decreases in the range from 170 to 150 nm, whereas with an increase in the feed rate of the electrospinning solution from 0.1 ml/h to 0.6 ml/h, the average diameter increases in the range of 137–157 nm. The uniformity of the diameter of nanofibers increases with decreasing the diameter of the needle and increasing the feed rate.

Influence of electrical voltage and distance between the needle and the substrate Nanofibers are obtained in a stable process with an electric voltage in the range of 17–30 kV and with a distance in the range of 60–150 mm, but at an electrical voltage of above 23 kV and at a distance of less than 90 mm, droplets can be observed. SEM images of obtained nanofibrillar membranes at various working distances between the tip of the needle and the substrate are shown in Fig. 1. Beads appear in nanofibers at a distance of 150 mm for low concentrations of the solution (solution 6) (see Fig. 1h and i). The average diameter of nanofibers versus the distance and electrical voltage is shown in Fig. 2f and g, from which it follows that the diameter of nanofibers decreases from 238 to 135 nm with an increase in the distance between the needle tip and the substrate from 60 to 150 mm, and it decreases from 213 to 133 nm with an increase in the electric voltage from 17 to 26 kV.

At an electric voltage of 29 kV, the diameter of nanofibers increases to 157 nm. This can be attributed to the rapid evaporation of the solvent at high voltages (27–30 kV), i.e., the rapid curing of fibers, which leads to the formation of thicker nanofibers. Because the drop density in the membrane was high at small distances and high voltages, the optimal parameters for obtaining high-quality membranes are an electrical voltage of 17–23 kV, a distance of 120–150 mm, a feed rate

of 0.1–0.3 ml/h, a needle diameter of 0.42–0.72 mm, and a material concentration of 47.4–41.39%.

Electrospinning solution properties

Solution properties (e.g., viscosity, surface tension, electrical conductivity) are important parameters that can dominate the morphology of nanofibers and the quality of membranes. To get a deep insight into the electrospinning process of CsPbI₃:PVP nanofibers, properties of used electrospinning solutions to prepare high-quality nanofibrillar membranes were determined. Describing the relationship between, on one hand, these properties and the mean diameter of nanofibers and, on the other hand, between the mean diameter and the properties of membranes allows preparing nanofibrillar membranes with predetermined properties that match the purpose of the preparation (solar cells, LEDs,

etc.). Also, these connections are important for preparing perovskite–polymer nanofibers based on various types of perovskites or polymers. Fig. S2 shows diagrams (viscosity–shear rate) and (shear stress–shear rate) for electrospinning solutions. According to results in Fig. S2, the relationship between the viscosity and the solution concentration is described in Fig. 3a.

We can notice that the viscosity increases with increasing PVP or perovskite amounts to change in the range of 198.56–2949.1 mPa.s with PVP and in the range of 130.48–296.41 mPa.s with perovskite. Furthermore, the viscosity increases with decreasing DMF amount to change in the range of 86.97–198.56 mPa.s. The relation between the electrical conductivity and the solution concentration is shown in Fig. 3b to change in the range of 7.26–8.44 mS/cm with DMF, 7.97–7.17 mS/cm with perovskite, and 7.26–5.4 mS/cm with PVP. In Fig. 3c, surface tension results were
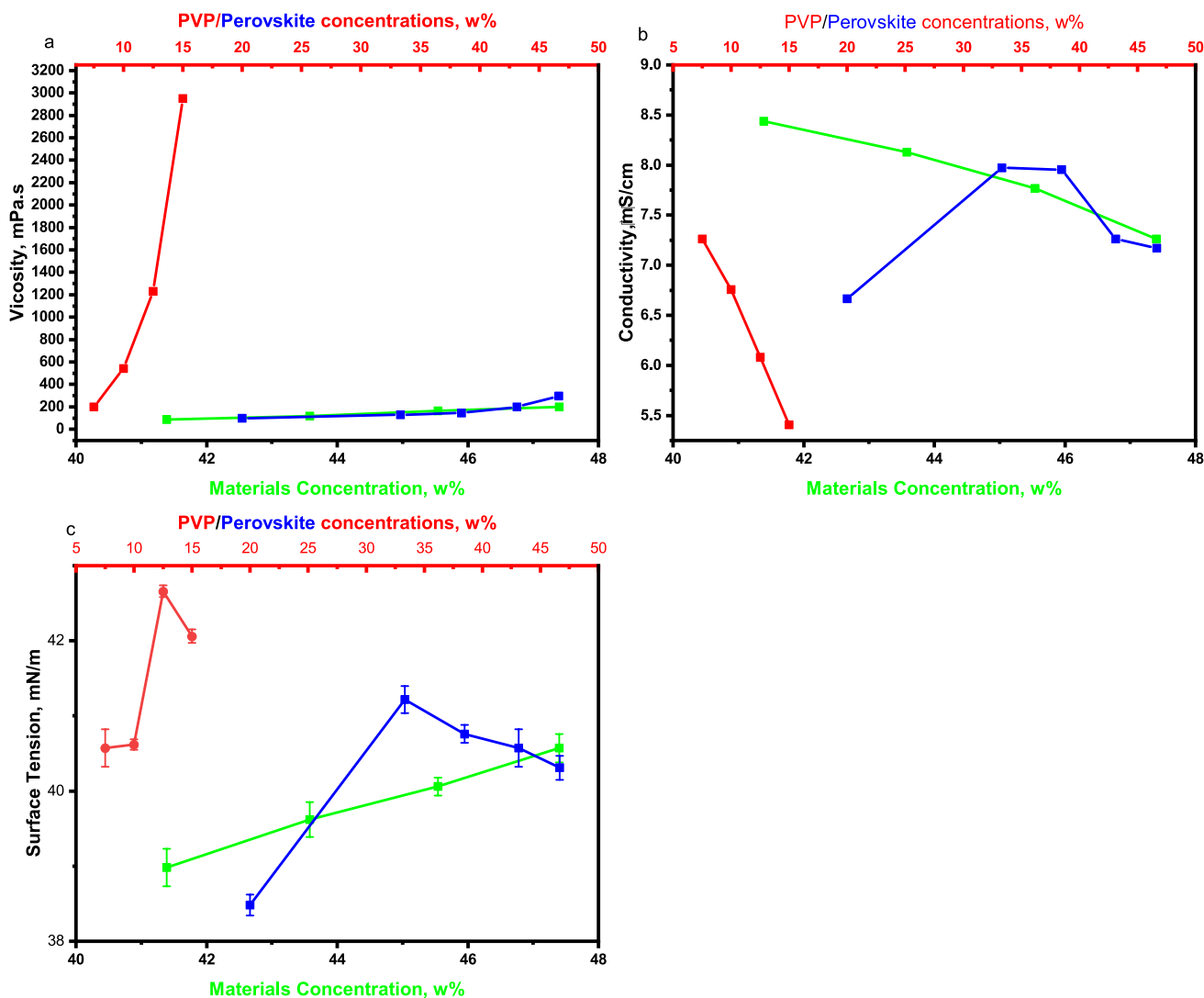

Fig. 3 Viscosity, electrical conductivity, and surface tension: solution concentration relationships

found to change in the range of 38.98–40.57 mN/m with DMF, 41.22–40.31 mN/m with perovskite, and 40.57–42.06 mN/m with PVP. Table S1 represents the change in the average diameter of nanofibers depending on the electrospinning solution properties. The analysis of presented results in Fig. 3 and Table 1 explains the high increase in the mean diameter of nanofibers at high concentrations of the polymer. An increase in the PVP amount leads to a sharp change in the properties of the electrospinning solution. In the case of perovskite, the change in the viscosity and conductivity is much less than that of PVP. It can be noticed that the viscosity and conductivity of electrospinning solutions manipulated based on perovskite and DMF are close. The increase in the average diameter of nanofibers at high perovskite concentrations (46.67%) can be attributed to a little increase in the viscosity, higher surface tension values than those of solutions based on DMF, and a decrease in the solution conductivity. The latter can be explained by the aggregation of ions, forming ionic clusters, which leads to a decrease in the mobility of charge carriers (Molinari et al. 2018; Kwak et al. 2003; Nithya et al. 2014; Meng et al. 2021). Actually, these ionic clusters play an important role in perovskite nucleation in nanofibers, which will be discussed later. Therefore, solution 3 was chosen for further study because it has low electrical conductivity (a high concentration of ionic clusters) without a significant increase in the average diameter of nanofibers.

Annealing process and perovskite crystallinity

After quality control of nanofibrillar membranes, an annealing process is required to form perovskite crystals into nanofibers. Samples were annealed at various temperatures and times. Figure 4a shows XRD patterns of membranes without annealing and annealed at temperatures of 60–350 °C for 5 min. There are no peaks in the XRD pattern of the membrane without annealing that can indicate the crystallinity of perovskite or semicrystalline regions of the polymer. The complexation between perovskites and PVP (as will be discussed in the IR results Fig. 4b) leads to a decrease in the intermolecular interaction between the polymer chains, increasing amorphous regions of the polymer (Nithya et al. 2014; Abdelrazek et al. 2018). As known, the phase transition to the black-phase α-CsPbI$_3$ occurs at an annealing temperature of about 350 °C. Sharp, high-intensity peaks indicate a highly crystalline, symmetrical perovskite structure. After annealing at temperatures from 250 °C to 300 °C, peaks become broader with the appearance of new peaks, indicating a distorted perovskite structure (lowered symmetry). The peak splitting at 28–29° characterizes the tetragonal structure of β-CsPbI$_3$ (Yao et al. 2021a). The gradual shift in peaks toward a larger diffraction angle can be observed by increasing

the temperature from 250 °C to 350 °C. This shift can be attributed to the lattice contraction (Wang et al. 2021d). At an annealing temperature above 150 °C, peaks at 14.25°, 20.29°, and 28.75° can be observed, indicating the formation of black-phase CsPbI$_3$. Actually, because of the low crystallinity, the identification of the phase type of CsPbI$_3$ after annealing at temperatures below 200 °C is considered a controversial issue for some researchers (Yi et al. 2020; Bansode et al. 2019; Haque et al. 2018). Although the optical properties deviate slightly from the ideal properties of α-CsPbI$_3$, Yi et al. registered it as γ-CsPbI$_3$ (Yi et al. 2020), Bansode et al. registered it as α-CsPbI$_3$ (Li et al. 2018; Bansode et al. 2019), while Haque et al. registered it as black-phase perovskite (Haque et al. 2018). To better understand the phase structure of the resulting perovskite after annealing below 200 °C, light absorption and PL spectra were recorded. Figure 4c shows the light absorption spectra of annealed samples at 150 °C and 200 °C for 5 min. Light absorption increases with increasing the annealing temperature from 150 °C to 200 °C, which is in agreement with the XRD results. Tauc plots of annealed samples at 150 °C and 200 °C for 5 min are shown in Fig. S3. Plots confirm the formation of black-phase CsPbI$_3$ with a bandgap (E$_g$) of ~ 1.77 eV and 1.74 eV at 150 °C and 200 °C, respectively. E$_g$ values agree well with other experimental results reported in the literature (Yi et al. 2020; Li et al. 2018; Bansode et al. 2019; Haque et al. 2018). PL spectra are shown in Fig. 4d. The PL intensity increases with an increase in the annealing temperature from 150 °C to 200 °C. For annealed samples at 150 °C and 200 °C, PL peaks are seen around 675 nm and 701 nm, which corresponds to a band gap of ~ 1.84 eV and 1.77 eV, respectively. Both light absorption and PL results show a shift towards lower values of the bandgap with increasing the annealing temperature, which is associated with an increase in grain size. The shift between E$_{optical}$ and E$_{emission}$ values could be attributed to the quantom size effect of NCs. As can be seen above, E$_g$ values of the obtained perovskite differ from the optimal value of α-CsPbI$_3$ (~ 1.73 eV). Therefore, we have decided to call the resulting perovskite phase after annealing at a temperature of below 200 °C for 5 min the black phase without specifying the type, whether it is the α or γ phase.

To evaluate the influence of annealing time on crystallinity, samples were annealed at 200–350 °C for 15 min. Results are shown in Fig. 4e. Increasing the annealing time at 350 °C from 5 to 15 min leads to a decrease in the intensity of peaks around (14.25°, 20.29°, 28.75°, 35.93°) of α-CsPbI$_3$. New peaks can be seen, which may be associated with the decomposition of perovskite. Whereas after 15 min of annealing at 200 °C, no changes were detected. Increasing
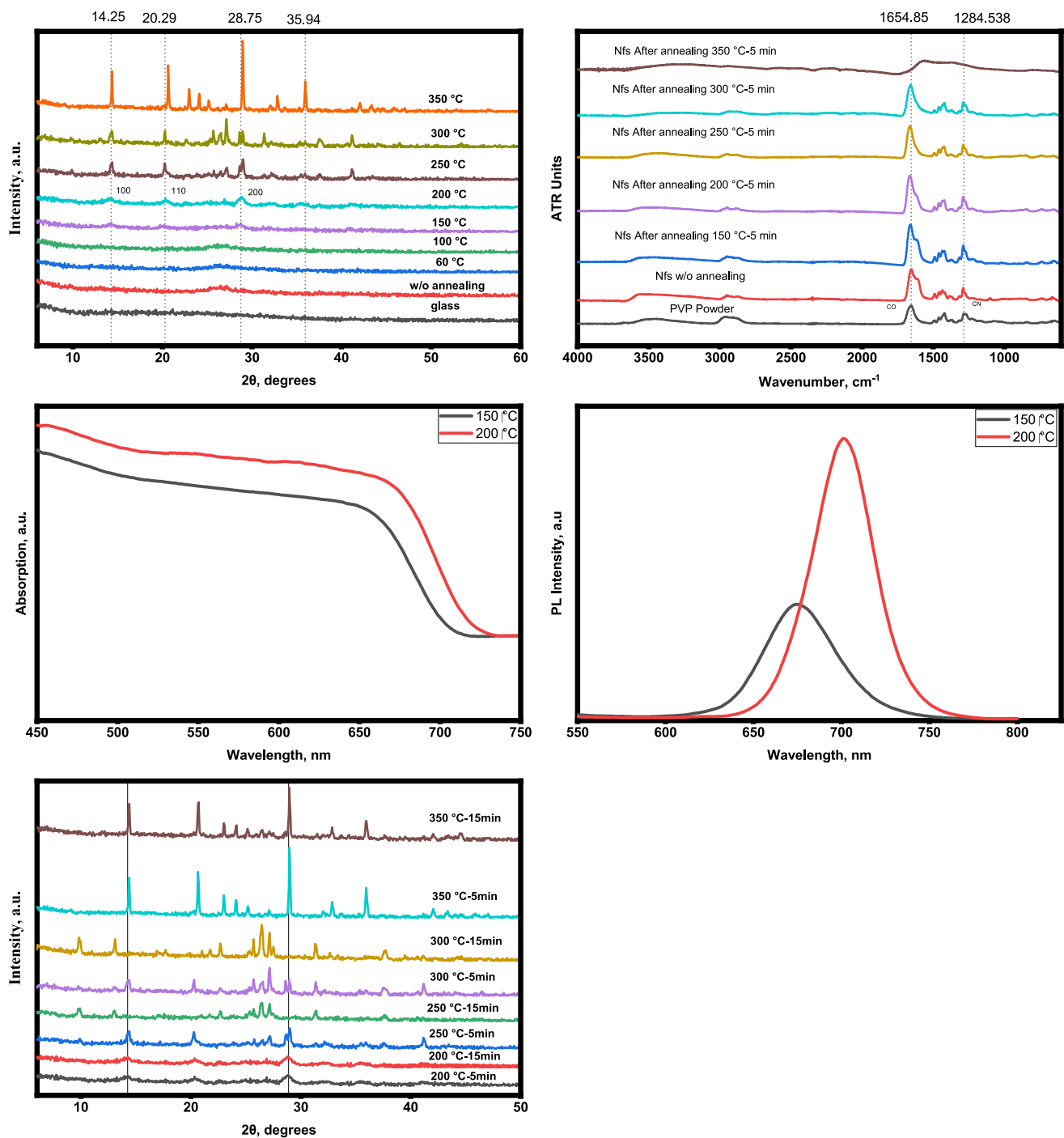
Fig. 4 a XRD patterns of annealed samples at temperatures of 60–350 °C for 5 min; **b** FTIR spectra of PVP powder, composite nanofibers after electrospinning, and after annealing at 150–350 °C for 5 min; **c** light absorption and **d** PL spectra of annealed samples at 150 °C and 200 °C for 5 min; **e** XRD patterns of annealed samples at 200 °C, 250 °C, 300 °C, 350 °C for 5 min and 15 min; at 200 °C,

no changes were detected; at 250 °C and 300 °C, the transformation of β-CsPbI$_3$ to δ-CsPbI$_3$ was observed; and at 350 °C, the intensity of the peaks around (14.25°, 20.29°, 28.75°, and 35.93°) of α-CsPbI$_3$ decreased. All samples were prepared under the following parameters: 23 kV voltage, 120 mm distance, 0.1 ml/h feed rate, solution 3

the annealing time from 5 to 15 min at 250 °C or 300 °C

leads to the transformation of β-CsPbI$_3$ to δ-CsPbI$_3$.

Structure of nanofibrillar membranes after annealing

Since our goal is to obtain flexible polymer nanofibers modified with perovskite NCs, it is critically important to study the effect of annealing parameters on the structure of nanofibers. Micrographs of samples before and after

annealing at 150–350 °C for 5–15 min are shown in Fig. S4–S6. Figure 5 shows SEM images of samples before and after annealing at 150 °C, 200 °C, 250 °C, 300 °C, and 350 °C for 5 min.

Membranes before annealing consist of main nanofibers decorated with thinner nanowires (Fig. 5a). After annealing at 150–200 °C for 5 min (Fig. 5b–c), a slight change in the membrane morphology can be observed. The average diameter of nanofibers somewhat decreases (Table 2).
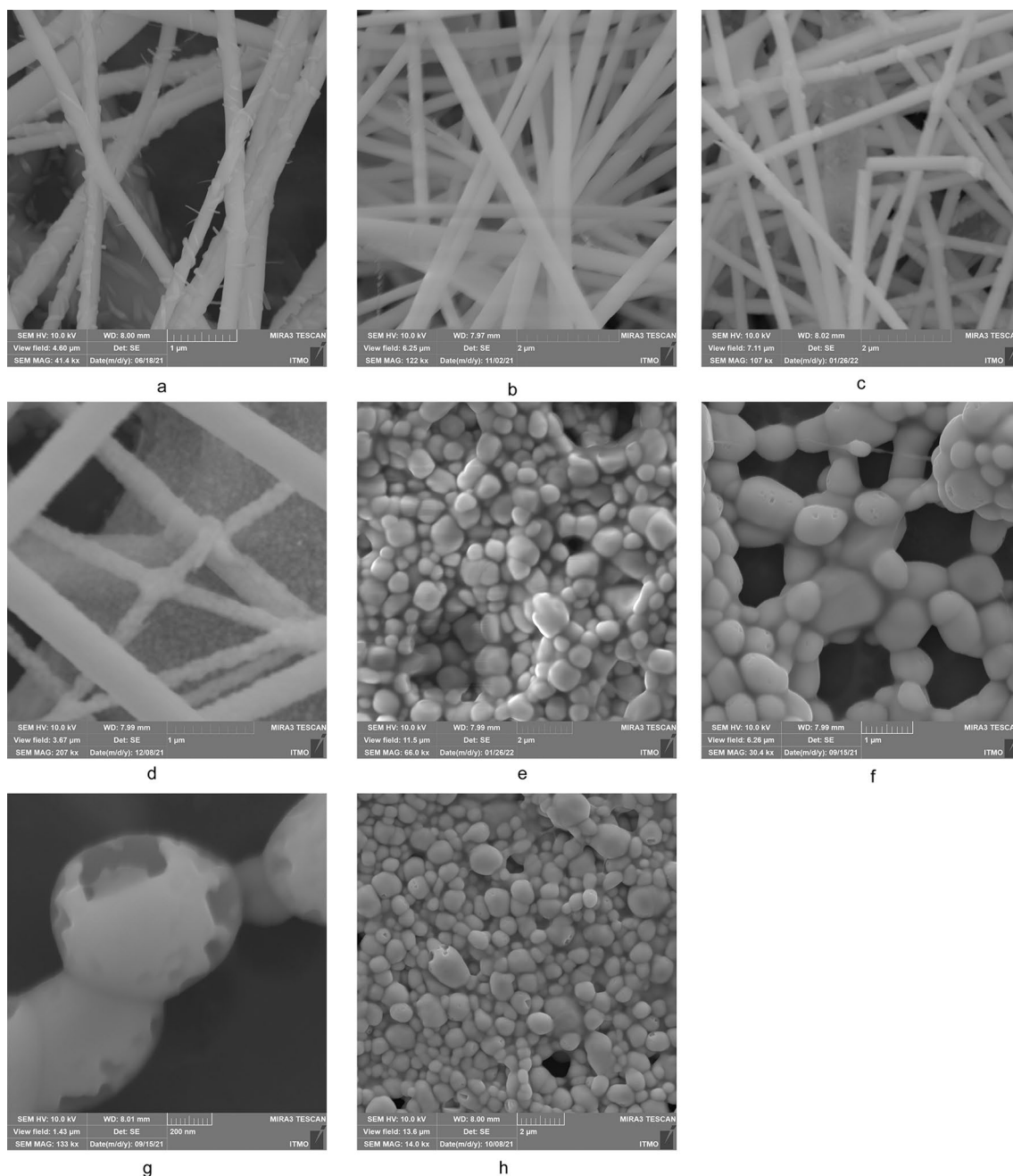

Fig. 5 Perovskite: PVP nanofibers before and after annealing. **a** Without annealing; **b** at 150 °C for 5 min; **c** at 200 °C for 5 min; **d** at 250 °C for 5 min; **e** at 300 °C for 5 min/solution 3; **f** at 350 °C for 5 min/solution 3; **g** at 350 °C for 5 min/solution 3; **h** at 350 °C for 5 min/solution 6

**Table 2** Influence of annealing conditions on the morphology of membranes

The average diameter of nanofibers before annealing	Electrospinning parameters	Annealing conditions	The average diameter of nanofibers/grains after annealing
228.82 ± 60 nm	23 kV voltage, 120 mm distance, 0.1 ml/h feed rate, 0.42 mm needle diameter, solution 3	200 °C for 5 min 300 °C for 5 min 350 °C for 5 min	Nanofibers: 209.5 ± 53 nm Grains: 719.86 ± 252 nm Grains: 769.51 ± 248 nm
168.51 ± 49 nm	20 kV voltage, 150 mm distance, 0.1 ml/h feed rate, 0.72 mm needle diameter, solution 6	350 °C for 5 min	Grains: 611.43 ± 205 nm

Nanofibers have become darker, and the nanowires are still observed. Perovskite crystals grow by increasing the annealing temperature, reducing the flexibility of nanofibers. After annealing at 250 °C for 5 min, parts of perovskite grains begin to appear on the surface of nanofibers (Fig. 5d). Increasing the annealing time from 5 to 15 min leads to the formation of nanofibers-shaped perovskite grains beginning at 250 °C (Fig. S6). After 5 min of annealing at 300–350 °C, nanofibers-shaped CsPbI$_3$ perovskite grains were obtained (Fig. 5e–h). The size of these grains is dependent on the annealing temperature and the average diameter of nanofibers (Table 2). For membranes with an average diameter of nanofibers of 229 nm, the average grain size was 769 nm, whereas with an average diameter of nanofibers of 168 nm, the average grain size was 611 nm. Thus, in addition to the annealing process, the grain size can be controlled by manipulating the diameter of nanofibers. In Fig. 5g, it can be seen that some polymer residues are on the surface of the grain and fill the gaps between them, making their edges opaque. Figure 6 schematically shows the change in the morphology of nanofibers with an increase in the annealing temperature. The nanostructure of nanofibers changes gradually from a nanofibrillar structure to nanofibers-shaped perovskite grains. As can be seen, the flexible nanofibrillar structure is preserved up to an annealing temperature of 200–250 °C.

So, to obtain flexible absorbers, the annealing temperature should not exceed this value. From Fig. 5, regardless of the annealing temperature, some pores between nanofibers or grains can be noticed. When these membranes are used in solar cells, pores can lead to short contacts between the hole and electron transport layers. These contacts contribute to a significant decrease in the device's current density and efficiency (Bkkar et al. 2022). Thus, manipulating the size of pores between nanofibers is crucial to avoid sacrificing the device's performance.

Mechanism of stable perovskite NCs' formation into polymer nanofibers

To explain the mechanism of perovskite NCs formation in polymer nanofibers, it is important to justify the presence of any interaction between PVP and perovskite before and after annealing since these interactions have a strong influence on the nucleation and crystallization of perovskite (Bkkar et al. 2022). Therefore, FTIR spectra of samples were recorded. Results are presented in Fig. 4b. Due to the basic nature of its functional groups, PVP is a good proton acceptor. From FTIR of composite membranes, it can be noticed that the broadness of the main peaks at (1654.85 cm^{-1}, CO) decreased, and a new peak as a shoulder appeared at
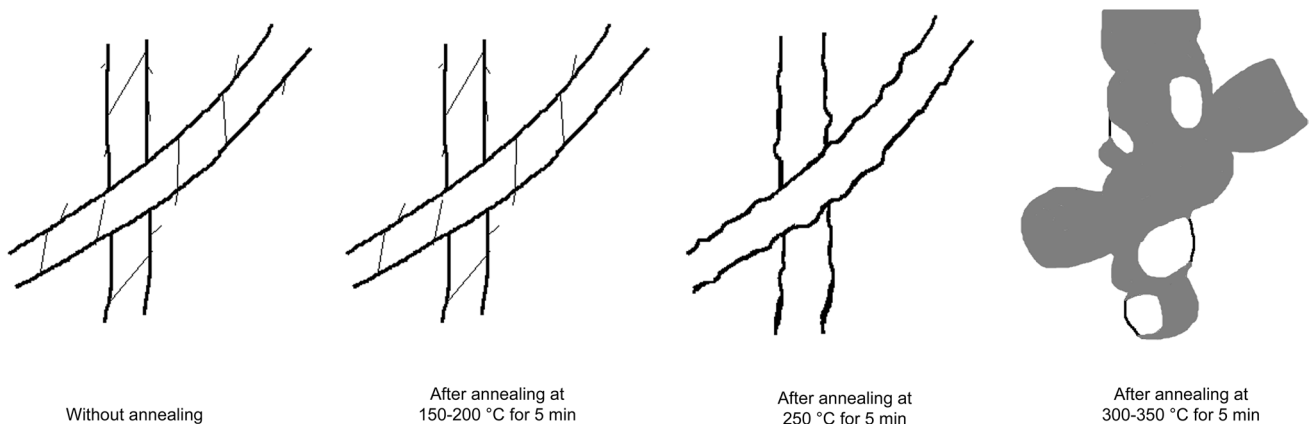
Fig. 6 A Schematic illustration of nanofibers' morphology before and after annealing

1610.7 cm^{-1}. This indicates a strong bond between the carbonyl group and the perovskite. The presence of perovskites (Lewis acids) leads to an increase in the basicity of the CO group (base Lewis) to behave as a strong electron donor. The intensity of this shoulder decreases with increasing the annealing temperature from 150 °C to 250 °C and disappears after annealing at 300 °C for 5 min. FTIR spectra of annealed samples at 200 °C for 5 min and 15 min are shown in Fig. S7. The complexation between PVP and perovskite was maintained with increasing annealing time up to 15 min.

The mechanism of NCs formation has been presented after confirming the interaction between PVP and perovskite. Figure 7a shows a schematic illustration of perovskite crystallization into nanofibers: (1) Perovskite precursors aggregate around solvent molecules and polymer chains (Lewis bases) in the electrospinning solution. Ionic clusters are formed in the solution as a result of the polymer and the high concentration of perovskite; (2) After electrospinning, the applied voltage and the large specific surface area lead to the fast evaporation of the solvent. As a result, perovskite precursors strongly aggregate around polymer chains, forming an intermediate phase. Covalent bonds are formed based on the Lewis acid–base approach. PVP's properties, such as containing donor atoms, dipole moment (2.2 D), and long polymer chains, cause it to act as a polymeric solvent for perovskites (Bkkar et al. 2022; Romiluyi et al. 2021; Kirakosyan et al. 2020). (3) Annealing promotes perovskite nucleation and crystal growth. The low annealing temperature can

be attributed to ionic clusters and the aggregation of perovskite precursors around polymer chains in the intermediate phase. The presence of PVP could lead to non-classical nucleation based on pre-nucleation clusters. These clusters formed by the interaction between the polymer and perovskites lower the Gibbs free energy barrier for nucleation (Meng et al. 2021; Zhang et al. 2020b; Gebauer and Colfen 2011). The complexation is formed between perovskite NCs and the polymer (Fig. 7b). Perovskite crystals grow gradually by increasing the annealing temperature or time. The nanofibrillar structure and PVP limit crystal growth (Bkkar et al. 2020, 2022). The density of free crystals (unrestricted by polymer chains) increases with an increase in the annealing temperature. So, after electrospinning, PVP acts as a host for perovskite precursors. Nuclei are formed on polymer chains and continue to grow complicated with them. Crystals are immobilized by the surrounding polymer chains as long as their size is smaller than the distance between polymer chains. With increasing the crystal size (the annealing temperature), the complexation between these crystals and PVP weakens.

Long-term stability of nanofibers

Figure S8 shows photographs of the fresh sample and photographs of samples after 15 min, 15 days, and 35 days from annealing at 60–350 °C for 5 min. All samples were stored at a room temperature of 27 °C and humidity of 21%. After
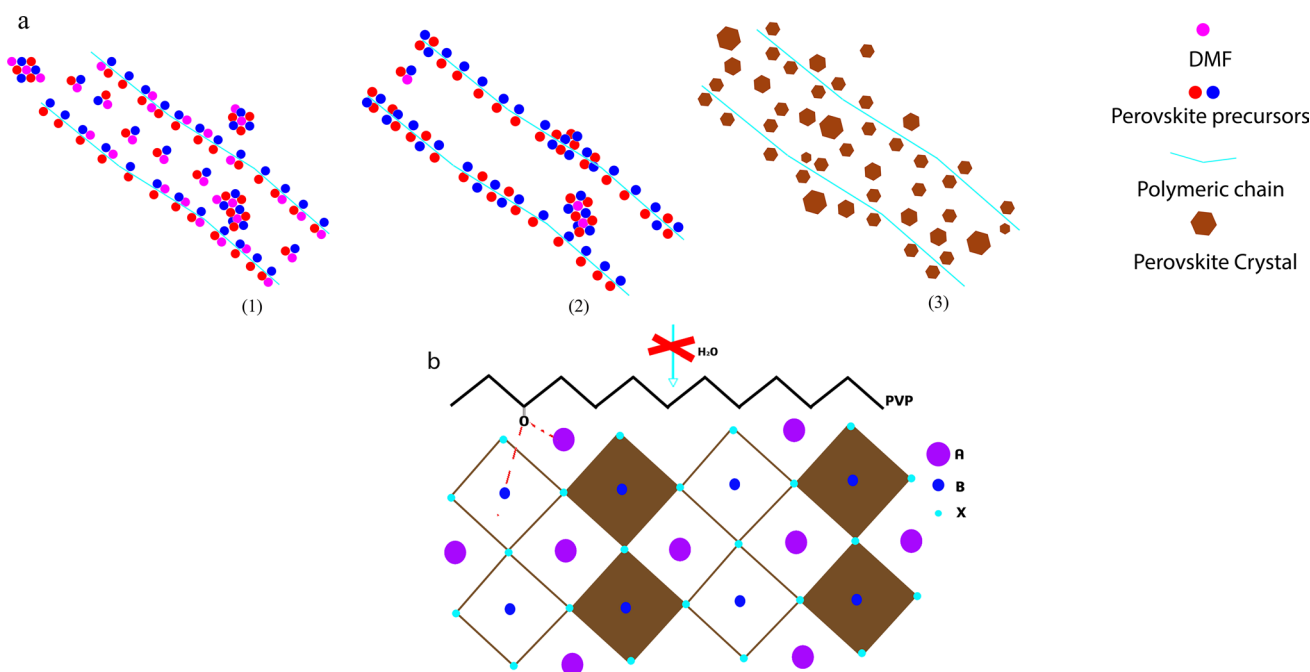

Fig. 7 **a** A Schematic illustration of perovskite crystallization: (1) electrospinning solution, (2) after electrospinning (fast solvent evaporation), (3) after annealing; **b** a schematic model of perovskite-polymer interactions

annealing, the color of samples turned black at 350 °C for 5 min or dark brown at 150–300 °C for 5 min. The change in the color can be explained by the phase transition of perovskite from the yellow phase to the black phase. After 15 min, the annealed sample at 300 °C for 5 min degraded to dark yellow with no change in the color for other annealed samples at 150 °C, 200 °C, and 250 °C for 5 min. After 15 days, the annealed sample at 250 °C for 5 min was degraded to brown–yellow faster than annealed samples at 150–200 °C, whereas the color of the annealed sample at 350 °C for 5 min changed to pale black. By changing the color of samples, we can say that annealed samples at 150 °C, 200 °C, and 350 °C for 5 min are more stable than others. To confirm the previous results, XRD patterns (Fig. 8a) for annealed samples at 200 °C and 350 °C for 5 min were recorded over time. Despite the black color of the sample annealed at 350 °C for 5 min, XRD patterns showed the degradation of perovskite from the α-perovskite to the δ-perovskite through 4 h. The black color can be explained by the PVP combustion and some residues of black perovskite. On the other hand, no

changes were observed in the X-ray diffraction pattern of the sample annealed at 200 °C for 5 min.

Figure 8b shows light absorption spectra of fresh, 15-day, and 35-day samples annealed at 200 °C for 5 min. Light absorption spectra of fresh and 15-day samples annealed at 250 °C for 5 min are shown in Fig. 8c. The annealed membrane at 200 °C for 5 min retained their light absorption properties for up to 15 days. The annealed membrane at 250 °C for 5 min lost a large part of its ability to absorb light after 15 days from the annealing moment. Stability results of annealed samples at 150–200 °C for 5 min can be explained by the passivating effect of PVP and the small size of crystals. The required crystal size to obtain a stable perovskite structure is achieved at an annealing temperature of about 200 °C. The presence of PVP limits the crystals' growth and passivates their surfaces. Based on FTIR spectra (Fig. 4b), it can be noticed that the passivation effect (perovskite–polymer complexation) reduces at an annealing temperature of 250 °C for 5 min and does not exist at an annealing temperature of 300 °C for 5 min. This explains the low stability of
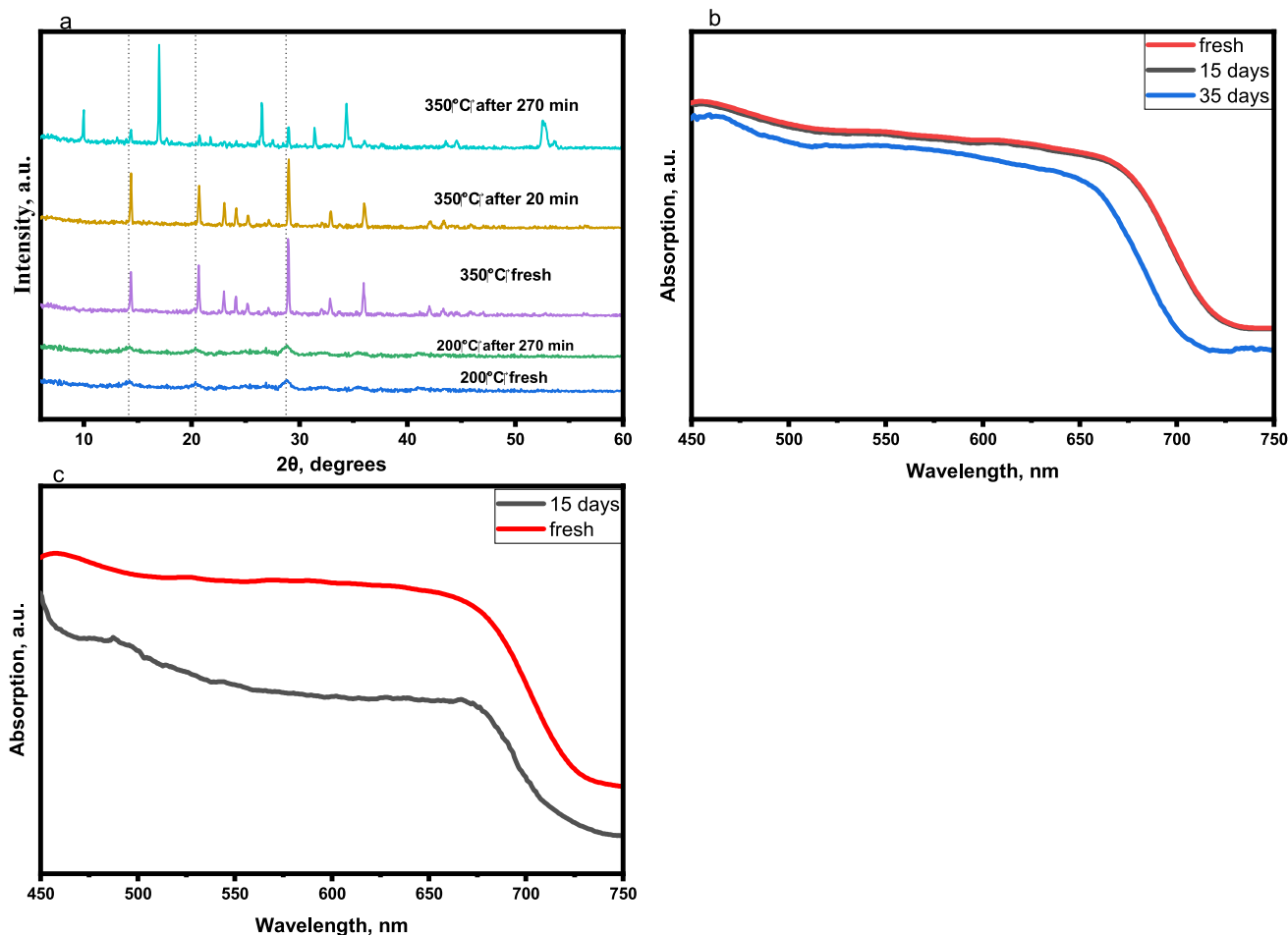

Fig. 8 **a** XRD patterns of fresh and 4-h samples after 5 min of annealing at 350 °C and 200 °C. Light absorption spectra of (**b**) fresh, 15-day, and 35-day samples after annealing at 200 °C for 5 min; (**c**) fresh and 15-day samples after annealing at 250 °C for 5 min

the annealed sample at 250 °C for 5 min and the instability at 300 °C for 5 min. In other words, to obtain flexible nanofibrillar membranes with an environmental stability of perovskite up to 15 days, the annealing temperature should achieve a compromise between the crystal size, the passivation effect, and the preservation of the nanofibrillar structure.

Based on the previous analysis, we can present the relationship between the structure of nanofibers and their stability. As long as perovskite grains are covered by the polymer within the nanofibrillar structure (annealing conditions: 150–200 °C for 5 min), black-phase CsPbI$_3$ remains stable for up to 15 days. When some parts of grains appear on the surface of nanofibers (annealing conditions: 250 °C for 5 min), the stability of CsPbI$_3$ drops significantly. Increasing the annealing time from 5 to 15 min at 250 °C and 300 °C leads to the formation of nanofibers-shaped perovskite grains, thus, the transformation of β-CsPbI$_3$ to δ-CsPbI$_3$ (see Fig. 4e and Fig. S6). Interestingly, although the formation of nanofibers-shaped perovskite grains after annealing at 350 °C for 15 min (compare Figs. 4e, 5 and S6), α-CsPbI$_3$ is still recorded, unlike annealed samples at 250 °C and 300 °C for 15 min.

Thermogravimetric analysis of nanofibers

A thermogravimetric analysis has been carried out to compare the thermal stability of PVP and PVP:CsPbI$_3$ nanofibers, as well as to study the thermal stability of samples over time at constant temperatures and the influence of the type of medium and temperature value on the thermal stability. In the case of PVP:CsPbI$_3$ nanofibers at a temperature growth rate of 25–900 °C in N$_2$ (Fig. 9a), it can be noticed that the thermal decomposition occurs in several stages. The first stage is PVP decomposition, with an extrapolated onset temperature of 419.76 °C (92.38%), followed by perovskite decomposition, with PbI$_2$ reaching 459.7 °C (85.2%) and CsI reaching 594.7 °C (80.1%). As a result, CsPbI$_3$:PVP nanofibers are thermally stable up to 300–420 °C with a weight loss of 95.4–92.3%. Pure PVP nanofibers are thermally stable up to 371.5 °C (79.3%) and begin to decompose at 291.5 °C (84.3%). At 200 °C, the weight loss is 96.5% for CsPbI$_3$:PVP nanofibers and 85.7% for PVP nanofibers. It can be seen that the thermal stability of PVP:CsPbI$_3$ nanofibers is higher than that of pure PVP nanofibers. This can be explained by the presence of perovskite.

To better understand the thermal stability of samples over time at constant temperatures, a thermogravimetric analysis of samples was conducted at constant temperatures of 300 °C and 350 °C (Fig. 9b). First the temperature increases up to 300 or 350 °C at a rate of 20 K/min (stage 1), and then the temperature remains constant until the end of the hour (stage 2). From Fig. 9b, we can notice that the decomposition rate is higher at 350 °C than at 300 °C. It is important to note that the greatest loss in the sample weight occurs in stage 1 (Table S2). Furthermore, the thermal decomposition is dependent on the temperature rather than on the medium (air or nitrogen). According to Fig. 9a, the weight loss of samples in stages 1 and 2 could be attributed to the solvent evaporation and polymer decomposition. The IR spectra of samples (Fig. S9) confirm the combustion of PVP after the
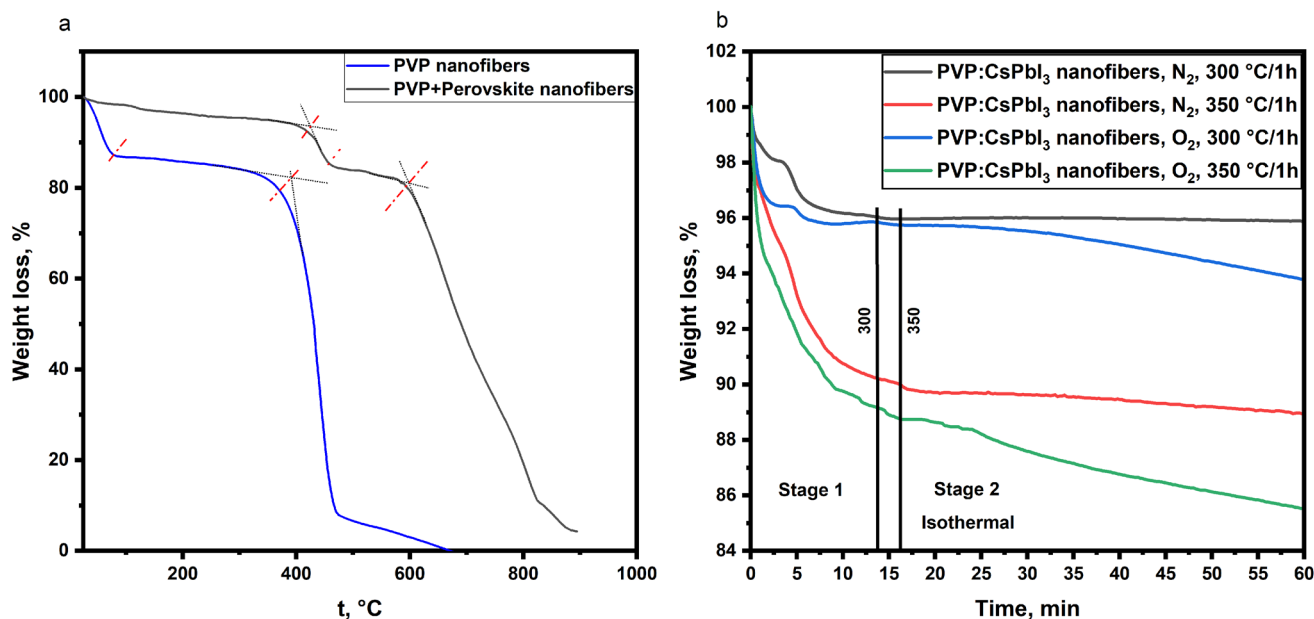

Fig. 9 A thermogravimetric analysis of fabricated nanofibers at (**a**) a thermal growth rate of 25–900 °C; (**b**) constant temperatures of 300 °C and 350 °C

thermal analysis at 300 °C or 350 °C in air for 1 h and the partial decomposition after the thermal analysis at 350 °C in inert nitrogen for 1 h. Finally, there are various factors that determine the thermal stability of PVP:CsPbI$_3$ nanofibers: 1. the thermal decomposition point of the component with the lowest thermal stability (in our case, PVP); 2. the compromise temperature that provides the optimal size of crystals while maintaining the bond between components (PVP and perovskite) and preserving the nanofibrillar structure. As we have seen from TGA results, the composite nanofibers are thermally stable up to 300–420 °C. Whereas, the compromise temperature was discovered to be up to 200 °C. Therefore, the working temperature of nanofibers should not exceed 200 °C.

Conclusion

The electrospinning process of CsPbI$_3$:PVP nanofibers has been studied. The influence of various parameters related to the electrospinning solution and setup on the quality of membranes was determined. There was no significant change in the average diameter of nanofibers at the following electrospinning parameters: a distance of 120–150 mm; a feed rate of 0.1–0.3 ml/h; and a needle diameter of 0.42–0.72 mm. The average diameter of nanofibers is strongly affected by the electrical voltage (17–23 kV) and the concentration of the solution. An increase in the PVP concentration from 7.5% to 15% leads to a sharp change in properties of the electrospinning solution, which leads to a strong increase in the average diameter of nanofibers. The formation of ionic clusters reduces the conductivity of the electrospinning solution as the concentration of perovskite increases from 33.33% to 46.67%. The latter contributes to the non-classical nucleation of perovskite, lowering the required annealing temperature for perovskite crystallization. The optimal annealing conditions were chosen at 200 °C for 5 min to preserve the complex formation between the polymer and perovskite, as well as the flexible nanofibrillar structure. Finally, flexible membranes with stable black-phase CsPbI$_3$ NCs were successfully prepared at room conditions. The operational temperature of these membranes is up to 200 °C, which is higher than other perovskites. The thermal analysis of nanofibers showed a slight weight loss of 3.5% of CsPbI$_3$:PVP nanofibers at a temperature of 200 °C. The flexibility and thermal stability of the resulting nanofibers make them potential candidates for flexible and stretchable optoelectronic applications. However, the investigation of the influence of electrospinning parameters on the crystallinity and optoelectronic properties is necessary to improve the quality of membranes and the stability of perovskite at room temperature. Furthermore, manipulating the size of pores between nanofibers is crucial to avoid sacrificing the performance of optoelectronic devices.

Declarations

References

Abdelrazek EM, Abdelghany AM, Badr SI, Morsi MA (2018) Structural, optical, morphological and thermal properties of PEO/PVP blend containing different concentrations of biosynthesized Au nanoparticles. J Market Res 7:419–431. https://doi.org/10.1016/j.jmrt.2017.06.009

Ahmadian A, Shafiee A, Aliahmad N, Agarwal M (2021) Overview of nanofiber mats fabrication via electrospinning and morphology analysis. Textiles 1:206–226. https://doi.org/10.3390/textiles1020010

Akkerman QA, Rainò G, Kovalenko MV, Manna L (2018) Genesis, challenges and opportunities for colloidal lead halide perovskite nanocrystals. Nat Mater 394(17):394–405. https://doi.org/10.1038/s41563-018-0018-4

Ava TT, Al Mamun A, Marsillac S, Namkoong G (2019) A review: thermal stability of methylammonium lead halide based perovskite solar cells. Appl Sci 9:188. https://doi.org/10.3390/app9010188

Bansode U, Rahman A, Ogale S (2019) Low-temperature processing of optimally polymer wrapped-CsPbI$_3$ for self-powered flexible photo-detector application. J Mater Chem C 7:6986–6996. https://doi.org/10.1039/c9tc01292c

Bkkar M, Olekhnovich RO, Uspenskaya M V (2020) Obtaining nanofibers based on perovskite-polymer composites for applying in solar cells. In Proceedings of International Multidisciplinary Scientific GeoConference: SGEM, Sofia, Bulgaria 20:129–136. https://doi.org/10.5593/sgem2020/4.1/s17.017

Bkkar MA, Olekhnovich RO, Uspenskaya MV (2022) Perovskite nanocomposite layers engineering for efficient and stable solar cells. J Nano Res 71:71–109. https://doi.org/10.4028/www.scientific.net/JNanoR.71.71

Bohr C, Pfeiffer M, Oz S, von Toperczer F, Lepcha A, Fischer T, Schutz M, Lindfors K, Mathur S (2019) Electrospun hybrid perovskite fibers—flexible networks of one-dimensional semiconductors for light-harvesting applications. ACS Appl Mater Interfaces 11:25163–25169. https://doi.org/10.1021/acsami.9b05700

Bohr C, Lê K, Fischer T, Mathur S (2022) Triaxial perovskite composite fibers spinning the way to flexible solar cells. Adv Eng Mater 24:2100773. https://doi.org/10.1002/adem.202100773

Borrotti M, Lanzarone E, Manganini F, Ortelli S, Pievatolo A, Tonetti C (2017) Defect minimization and feature control in electrospinning through design of experiments. J APPL POLYM SCI 134:17. https://doi.org/10.1002/APP.44740

Cao B, Yang L, Jiang S, Lin H, Wang N, Li X (2019) Flexible quintuple cation perovskite solar cells with high efficiency. J Mater Chem A 7:4960–4970. https://doi.org/10.1039/c8ta11945g

Chen D, Zhu Y (2017) Electrospun perovskite nanofibers. Nanosc Res Lett 12:1–5. https://doi.org/10.1186/s11671-017-1856-8

Chen T, Huang M, Ye Z, Hua J, Lin S, Wei L, Xiao L (2021) Blinking CsPbBr3 perovskite nanocrystals for the nanoscopic imaging of electrospun nanofibers. Nano Res 14:1397–1404. https://doi.org/10.1007/s12274-020-3189-7

Ding B, Yu J (2014) Electrospun nanofibers for energy and environmental applications. Springer, New York

Gebauer D, Colfen H (2011) Prenucleation clusters and non-classical nucleation. Nano Today 6:564–584. https://doi.org/10.1016/j.nantod.2011.10.005

Haider A, Haider S, Kang I-K (2018) A comprehensive review summarizing the effect of electrospinning parameters and potential applications of nanofibers in biomedical and biotechnology. Arab J Chem 11:1165–1188. https://doi.org/10.1016/j.arabjc.2015.11.015

Haque F, Wright M, Mahmud MA, Yi H, Wang D, Duan L, Xu C, Upama MB, Uddin A (2018) Effects of hydroiodic acid concentration on the properties of CsPbI$_3$ perovskite solar cells. ACS Omega 3:11937–11944. https://doi.org/10.1021/acsomega.8b01589

He J-H, Liu Y, Mo L-F, Wan Y-Q, Xu L (2008) Electrospun nanofibres and their applications. ISmithers Shawbury, UK.

Kim H-J, Oh H, Kim T, Kim D, Park M (2022) Stretchable photodetectors based on electrospun polymer/perovskite composite nanofibers. ACS Appl Nano Mater 5(1):1308–1316. https://doi.org/10.1021/acsanm.1c03875

Kirakosyan A, Kim Y, Sihn MR, Jeon M-G, Jeong J-R, Choi J (2020) Solubility-controlled room-temperature synthesis of cesium lead halide perovskite nanocrystals. ChemNanoMat 6:1863–1869. https://doi.org/10.1002/cnma.202000471

Kwak G-H, Tominaga Y, Asai S, Sumita M (2003) AC complex impedance measurement of comb-like type polyether electrolytes under high-pressure carbon dioxide. Electrochim Acta 48:4069–4075. https://doi.org/10.1016/S0013-4686(03)00564-4

Li B, Zhang Y, Fu L, Yu T, Zhou S, Zhang L, Yin L (2018) Surface passivation engineering strategy to fully-inorganic cubic CsPbI$_3$ perovskites for high-performance solar cells. Nat Commun 9:1076. https://doi.org/10.1038/s41467-018-03169-0

Li G, Jiang Z, Wang W, Chu Z, Zhang Y, Wang C (2019) Electrospun PAN/MAPbI$_3$ composite fibers for flexible and broadband photodetectors. Nanomaterials 9:50. https://doi.org/10.3390/nano9010050

Liu M, Jiang N, Huang H, Lin J, Huang F, Zheng Y, Chen D (2021) Ni^{2+}-doped CsPbI$_3$ perovskite nanocrystals with near-unity photoluminescence quantum yield and superior structure stability for red light-emitting devices. Chem Eng J 413:127547. https://doi.org/10.1016/j.cej.2020.127547

Masi S, Gualdron-Reyes AF, Mora-Sero I (2020) Stabilization of black perovskite phase in FAPbI$_3$ and CsPbI$_3$. ACS Energy Lett 5:1974–1985. https://doi.org/10.1021/acsenergylett.0c00801

Meng X, Li Y, Qu Y, Chen H, Jiang N, Li M, Xue D-J, Hu J-S, Huang H, Yang S (2021) Crystallization kinetics modulation of FASnI$_3$ films with pre-nucleation clusters for efficient lead-free perovskite solar cells. Angew Chem Int Ed 60:3693–3698. https://doi.org/10.1002/anie.202012280

Miyasaka T, Kulkarni A, Kim GM, Oz S, Jena AK (2020) Perovskite solar cells: can we go organic-free, lead-free, and dopant-free. Adv Energy Mater 10:1902500. https://doi.org/10.1002/aenm.201902500

Molinari N, Mailoa JP, Kozinsky B (2018) Effect of salt concentration on ion clustering and transport in polymer solid electrolytes: a molecular dynamics study of PEO–LiTFSI. Chem Mater 30:6298–6306. https://doi.org/10.1021/acs.chemmater.8b01955

Nithya S, Selvasekarapandian S, Karthikeyan S, Inbavalli D, Sikkinthar S, Sanjeeviraja C (2014) AC impedance studies on proton-conducting PAN:NH$_4$SCN polymer electrolytes. Ionics 20:1391. https://doi.org/10.1007/s11581-014-1091-6

Patil JV, Mali SS, Hong CK (2020) Boosting the stability of fully-inorganic perovskite solar cells through samarium doped CsPbI$_2$Br perovskite. ACS Sustain Chem Eng 8:16364–16371. https://doi.org/10.1021/acssuschemeng.0c06452

Romiluyi O, Eatmon Y, Ni R, Rand BP, Clancy P (2021) The efficacy of Lewis affinity scale metrics to represent solvent interactions with reagent salts in all-inorganic metal halide perovskite solutions. J Mater Chem A 9:13087–13099. https://doi.org/10.1039/D1TÄ3A

Sarac AS (2017) Nanofibers of conjugated polymers. CRC Press

Sun Y, Zhang H, Zhu K, Ye W, She L, Gao X, Ji W, Zeng Q (2021) Research on the influence of polar solvents on CsPbBr3 perovskite QDs. RSC Adv 11:27333. https://doi.org/10.1039/d1ra04485k

Tsai P-C, Chen J-Y, Ercan E, Chueh C-C, Tung S-H, Chen W-C (2018) Uniform luminous perovskite nanofibers with color-tunability and improved stability prepared by one-step core/shell electrospinning. Small 14:1704379. https://doi.org/10.1002/smll.201704379

Tumusange MS, Subedi B, Chen C, Junda MM, Song Z, Yan Y, Podraza NJ (2021) Impact of humidity and temperature on the stability of the optical properties and structure of MAPbI$_3$, MA$_{0.7}$ FA03PbI$_3$ and (FAPbI$_3$)$_{0.95}$ (MAPbBr$_3$)$_{0.05}$ perovskite thin films. Materials 14:4054. https://doi.org/10.3390/ma14144054

Wang K, Jin Z, Liang L, Bian H, Bai D, Wang H, Zhang J, Wang Q, Liu S (2018) All-inorganic cesium lead iodide perovskite solar cells with stabilized efficiency beyond 15%. Nat Commun 9:4544. https://doi.org/10.1038/s41467-018-06915-6

Wang Y, Yokota T, Someya T (2021a) Electrospun nanofiber-based soft electronics. NPG Asia Mater 13:1–22. https://doi.org/10.1038/s41427-020-00267-8

Wang S, Amin AAY, Wu L, Cao M, Zhang Q, Ameri T (2021b) Perovskite nanocrystals: synthesis, stability, and optoelectronic applications. Small Struct 2:2000124. https://doi.org/10.1002/sstr.202000124

Wang R, Zhang H, Han S, Wu Y, Hu Z, Zhang G, Liu H, He Q, Zhang X (2021c) Cadmium doping for improving the efficiency and stability of carbon-based CsPbIBr2 all inorganic perovskite solar cells. New J Chem 45:9243–9250. https://doi.org/10.1039/d0nj06317g

Wang M, Ni Z, Xiao X, Zhou Y, Huang J (2021d) Strain engineering in metal halide perovskite materials and devices: influence on stability and optoelectronic properties. Chem Phys Rev 2:031302. https://doi.org/10.1063/5.0044588

Yao Z, Zhao W, Liu SF (2021a) Stability of the CsPbI$_3$ perovskite: from fundamentals to improvements. J Mater Chem A 9:11124–11144. https://doi.org/10.1039/d1ta01252e

Yao H, Zhao J, Li Z, Ci Z, Jin Z (2021b) Research and progress of black metastable phase CsPbI$_3$ solar cells. Mater Chem Front 5:1221–1235. https://doi.org/10.1039/d0qm00756k

Yi C, Liu C, Wen K, Liu X-K, Zhang H, Yu Y, Fan N, Ji F, Kuang C, Ma B et al (2020) Intermediate-phase-assisted low-temperature formation of γ-CsPbI$_3$ films for high-efficiency deep-red light-emitting devices. Nat Commun 11:4736. https://doi.org/10.1038/s41467-020-18380-1

Zhang Q, Deng X, Tan C, Zhou Y, Chen X, Bai X, Li J, Tang B, Li S, Lin H (2020a) Gamma-phase CsPbBr3 perovskite nanocrystals/polymethyl methacrylate electrospun nanofibrous membranes with superior photo-catalytic property. J Chem Phys 153:024703. https://doi.org/10.1063/5.0012938

Zhang K, Wang Z, Wang G, Wang J, Li Y, Qian W, Zheng S, Xiao S, Yang S (2020b) A prenucleation strategy for ambient fabrication of perovskite solar cells with high device performance uniformity. Nat Commun 11:1006. https://doi.org/10.1038/s41467-020-14715-0